VOL. 7, NO. 4, APRIL 2012 ISSN 1819-6608
ARPN Journal of Engineering and Applied Sciences
©2006-2012 Asian Research Publishing Network (ARPN). All rights reserved.

www.arpnjournals.com

SECONDARY FLOW LOSSES BEHIND A GEOMETRICAL DESIGNED FOUR TURBINE BLADE CASCADE

Ali S. Abass and A. I. Noor Y. Abass
Department of Mechanical Engineering, Al Nahrain University, Baghdad, Iraq
E-Mail: alisabass@gmail.com

ABSTRACT

The present study define the turbine blade characteristics starting from blade geometry design and continued through an investigation of wake flow generated downstream of blade cascade in a certain boundary conditions. Design of blade geometry was attained by employing of mathematical techniques namely called rapid axial turbine design, RATD. The modified aerodynamic optimization process was used in order to obtain an efficient and reliable optimization blade shape obtained from RATD technique. The wake characteristic was observed by introducing experimental work inside a test rig. This rig consists of rectangular wind tunnel with four blades cascade constructed locally with blade shape adopted from present blade design theory. The wake domain was tested downstream of the blade cascade by aid of five-hole probe for pressure measurements with a pitch angles ranged between -30 and 30 degree in the normal plane direction while the yaw angles was ranged between -30 and 30 degree in the axial plane direction. The total pressure coefficient (Cp_t) found to manifest a region of wake propagating starts from the end of wake center at suction surface to almost twice chord length towards downstream direction with a pitch distance equals to half, while at same time another wake region occur at downstream distance of 1.3 of chord length with a 0.75 pitch. These high loss regions represented by appearing of high regions for total pressure loss coefficients vary between 1.7 and 1.9 are caused by secondary flow vortices such as passage vortex which is converted via midspan. It was concluded that the positions of maximum static loss coefficient behavior reveals same level for all downstream axial distance, which results in better performance than Langston model.

Keywords: secondary flow, wake flow, turbine blade cascade.

INTRODUCTION

Blade design geometry

Aerodynamic shape optimization of three dimensional turbine blades involves the determination of the blade profile that will provide the best aerodynamic performance in a specified flow environment. A proper representation of the blade profile becomes essential for an efficient and successful optimization strategy. In turbo machinery, a 3D blade profile is usually defined in terms of three to seven 2D blade sections which are stacked in the spanwise direction and are blended together from hub to shroud. It is usual to deal with a set of traditional geometric design parameters that used to model the 2D airfoils such as leading and trailing edge radii, blade angles, wedges angles, axial and tangential chords, throat etc. However, these design parameters cannot be implemented into an optimization procedure unless they are implicitly enforced into the geometric representation of the blade. The coefficients of such representation are used as design variables in the aerodynamic optimization problem while the designer parameters give the designer an insight as to how these parameters affect the design space. The combination of these two characteristics should provide a better matching between the design variables and the cost function, which would enhance the optimization process [1].

Furthermore due to the very high stresses they must endure the extremely high temperatures from the combustor, designers sometimes end up with very convoluted blade designs. It is a challenge to successfully formulate a representation that is simple and yet highly flexible to allow an aerodynamic shape optimizer to explore efficiently all possible regions of the design space.

The rapid axial turbine design algorithm (RATD) method showed some exemplary work on attempting to elaborate a simple yet flexible geometric representation of turbine blades using traditional design parameters and introduced in the present study as an eleven parameters technique (RATD) [2]. Of the 25 (or more) unique variables that can be associated with every aerofoil, only eleven are independent parameters. Furthermore only five variables need to be known at the start of a design, because default values can be used for the other six the axial chord, for example, must be carefully controlled by the aerodynamicist during the design of a turbine. But if the axial chord is initially unknown it can be estimated by assuming zero incidences, zero deviation, and requiring the incompressible Zweifel loading coefficient [2]. The tangential chord, on the other hand, is established from examining the surface velocity distributions. Moreover, and before going in describing results of RATD model, the six independent variables should be clarified first in order to have a complete lucid structure for the design procedure pertained to RATD model. The axial chord for example, must be carefully controlled during the design of a turbine. But if the axial chord is initially unknown it can be estimated by assuming zero incidence, zero deviation, and requiring incompressible Zweifel loading coefficient [2] to be 0.8. In this case, the default value is triggered by setting the parameter to zero. The tangential chord, on the other hand is established from examining the surface velocity distributions [3]. However, a good first guess comes from specifying the percent maximum thickness- to- chord, or

©2006-2012 Asian Research Publishing Network (ARPN). All rights reserved.

the axial chord and stagger angle, or by requiring that the rates of change of auction surface blade angle with axial distance be constant, set the cord thickness distribution equal to zero [4]. The unguided turning can be determined by requiring the suction surface second derivative to be continuous at throat. Next, the sequence of solving required specifying the percent blockages instead of selecting leading edge or trailing edge radii. Finally, if the throat is not well known, its default value comes from the blocked throat-to-pitch rule. Basically (RATD) start with breaks down the blade into five distinct regions composed of the leading and trailing edge arcs, the suction and pressure side surfaces both modeled with a cubic polynomial and a circular arc for the uncovered part of the blade suction surface. With the eleven parameters, it is possible to determine the locations of the five key points which represent intersection points between the five key points. The mathematical derivation and The FORTRAN Power Station package was employed to simulate the theoretical analysis. This Fortran Power Station code was found of a comprehensive but easy to use geometry model for axial flow turbine nozzles and rotors. The model used here is only useful for getting a good initial blade profile but not an aerodynamic shape optimization. The first step in any optimization procedure is to determine a good initial airfoil in order to initialize the aerodynamic optimization process. Therefore, an adequate turbine airfoil geometry model is crucial in order to have an efficient and reliable optimization process. The five key points are shown in Figure-1 and can be computed from the eleven independent parameters using the equations given in [4]. The optimum blade profile was obtained by using of 2BG program shows (Rapid Axial Turbine Design Algorithm), has been written using FORTRAN 90. Note that the exit half-wedge angle is a dependent variable that must be iterated upon to remove the suction surface throat point discontinuity. A good first guess at the exit half-wedge angle is one-half the unguided turning as shown in Figure-2.

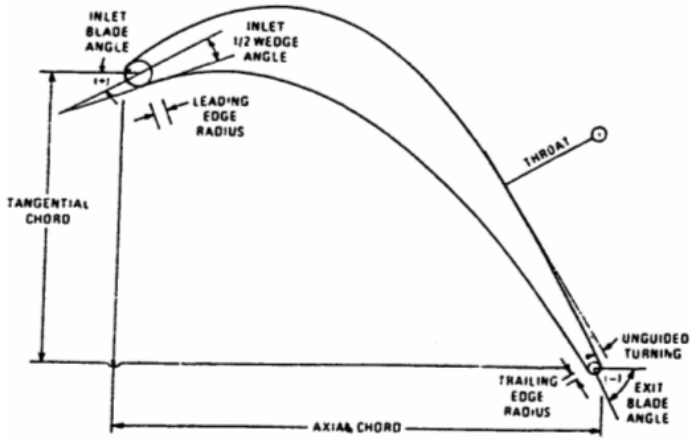

Figure-1. Schematic description of blade geometry.

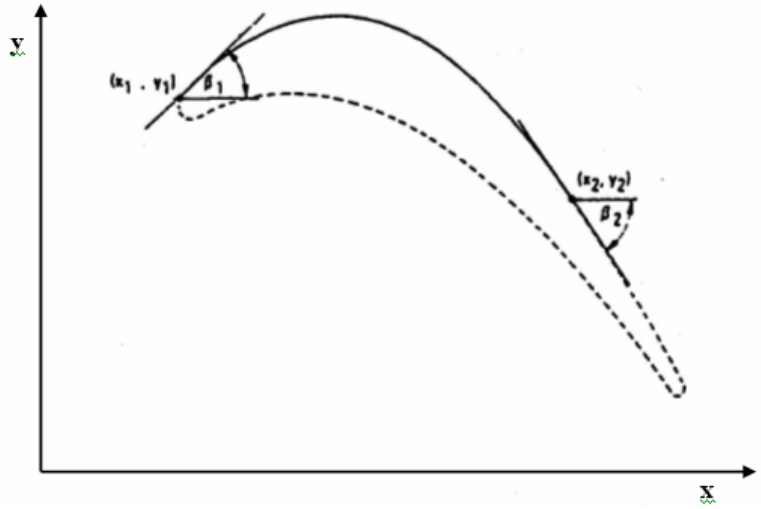

Where

$d\beta/dx$ = constant
x = x - axis for a point on blade camber line
y = ordinate
β_1 = inlet blade angle
β_2 = outlet blade angle.

Figure-2. Arc obtained from two points and two slopes.

©2006-2012 Asian Research Publishing Network (ARPN). All rights reserved.

In order to complete the airfoil description, the five key points must be connected. And the most convenient way to connect them is by five mathematical functions. Logical choices for three of these functions are a leading edge circle, a trailing edge circle, and a circular arc describing the uncovered suction surface past-the throat. The suction surface from the leading edge tangency point to the throat and the entire pressure surface of the airfoil were both defined by third order polynomials. Note that the cubic mathematical function is the most straightforward because it provides four simple algebraic equations and four unknown coefficients.

The blade final optimized shape of (RATD) model found resemble to Langston blade shape [5] in many basic points such as third polynomial curves on the suction surface from the leading edge tangency point to the throat, the entire pressure surface of the aerofoil besides leading edge circle, trailing edge circle, and circular arc describing the uncovered suction surface past the throat. Fugare-3 shows comparisons between (RATD), Langston and Parabolic Are Camber Line Method (PACLM) blade shapes. Both (RATD) and Langston blade shape are presented as the sold line blade in this Figure, while the dashed line blade represent the (PACLM) blade shape. Therefore, the (RATD) technique performs the most genuine representation for a turbine blade shape in comparison to other techniques, such as (PACLM), that reveals significant disagreements at the suction and pressure surface with (RATD) and Langston blade shapes. It is also concluded that varying of tangential chord, axial chord, leading edge radius, and the inlet blade angle illustrate a reasonable change in the standard shape of RATD (i.e., Langston model).

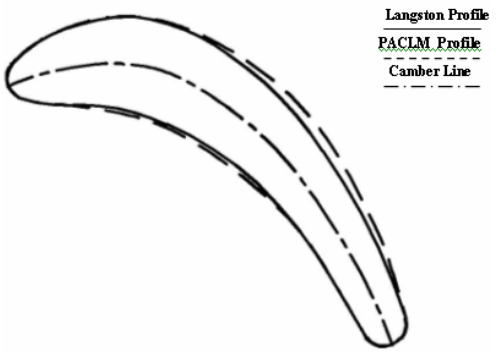

Figure-3. Comparison between present (PACLM) blade shape and langston blade [8].

EXPERIMENTAL SET UP

The experimental works were employed in this study to investigate the effect of wake flow on the flow characteristics parameters. These experiments were done in a laboratory under atmospheric condition. Experimental work was performed on a five linear cascade of an axial turbine blade consist of two end walls between which the constant section blades are placed as shown in Figure-4. The blade geometry adopted in the present work are the optimized blade shape obtained from (RATD) method in which it is approximately similar to those used by Langston in order to make a fair comparison between a previous well-known data with that of the experimental configurations. The experimental test rig includes the following parts:

a) Forced airflow system, which contains a centrifugal blower fan.
b) Manual control gate to maintain the proper volumetric flow rate throughout the passage of test rig.
c) Test section consists of five blades distributed at equal pitch distance to form a linear blade cascade of an axial turbine.
d) Pressure, velocity and temperature measurement apparatuses.

The blade geometry scaled by one-four of Langston blade in order to be convenient with the requirements of the present wind tunnel. Dimensions and angles for this blade cascade are shown as follows:

Number of blades = 5, Chord (mm) = 67, Axial chord (mm) = 62, Blade stagger angle = 24^0, Pitch (mm) = 60.47, Span (mm) = 61.2, Inlet flow angle = 44.7^0, Blade inlet angle = 43.99^0, Blade outlet angle = 25.98^0.

Figure-4. Blade row attached to one side of end wall.

Five-hole probe

A five-hole probe was used to measure the flow field downstream of the blade cascade. The easiest method of construction was chosen resulting in a forward-facing pyramid structure as defined by [6]. The five-hole probe was calibrated so that it could measure flows with a velocity direction oriented ± 30 degrees to the probe tip in both the yaw and pitch directions. The probe is calibrated at the duct test section in both yaw and pitch planes. Since there is no remarkable effect of the Reynolds number variation but only weakly influence has been found by Bosnian and Highton [7]. The ambient temperature and atmosphere pressure were 308 K and 1.023 bars respectively during the experimental program. Therefore; the calibration procedure is done as given by Charley [8]. The pressure reading may be averaged by using the relation given by Barker and Gallington [10]. The calibration coefficient maps for the probe can be found independently from the wind speed, because the

©2006-2012 Asian Research Publishing Network (ARPN). All rights reserved.


coefficients are non-dimensional. In order to assure accurate readings at low speeds and to investigate Reynolds number effects, the probe was calibrated at speed of 20 m/s. Therefore; the calibration procedure is done as given by Charley [8]. The pressure reading may be averaged by using the relation given by Barker and Gallington [10]. The estimated precision of five-hole probe measurement was as given by Sitaram [9]. The stem was clamped in a rotary jig that allowed precise rotation about yaw and pitch angles in 3-degree intervals.

Five-hole probe

A five-hole probe was used to measure the flow field downstream of the blade cascade. The easiest method of construction was chosen resulting in a forward-facing pyramid structure as defined by [6]. The five-hole probe was calibrated so that it could measure flows with a velocity direction oriented ± 30 degrees to the probe tip in both the yaw and pitch directions. The probe is calibrated at the duct test section in both yaw and pitch planes. Since there is no remarkable effect of the Reynolds number variation but only weakly influence has been found by Bosnian and Highton [7]. The ambient temperature and atmosphere pressure were 308 K and 1.023 bars respectively during the experimental program. Therefore; the calibration procedure is done as given by Charley [8]. The pressure reading may be averaged by using the relation given by Barker and Gallington [10]. The calibration coefficient maps for the probe can be found independently from the wind speed, because the coefficients are non-dimensional. In order to assure accurate readings at low speeds and to investigate Reynolds number effects, the probe was calibrated at speed of 20 m/s. Therefore; the calibration procedure is done as given by Charley [8]. The pressure reading may be averaged by using the relation given by Barker and Gallington [10]. The estimated Precision of five-hole probe measurement was as given by Sitaram [9]. The stem was clamped in a rotary jig that allowed precise rotation about yaw and pitch angles in 3-degree intervals.

Definition of angles and coordinates

In order to use the data collected with the probe correctly it was essential to define a coordinate system that was to be used in the calibration and the application later on. In all cases the positive x-direction was pointing in the direction of flow, z was pointing up and y was adjusted so the coordinate system was following the right hand rule.

During the calibration, all pressures P1 to P5 from the five-hole probes as well as P_{total} and $P_{dynamic}$ from the Pitot static tube are known, so that the pressure coefficient maps can be created. Ideally, the maps for the angles and pressure coefficients should show straight lines and concentric circles, respectively. The maps are useful devices to check the quality of the calibration and the degree of uncertainty from the ideal case [9].

Set-up of five-hole probe calibration

Calibration results obtained from pervious sections regarding coefficients of yaw angle, pitch angle, dynamic and total pressure were compared with the data obtained by [6]. Acceptable agreement was found between the two calibration results, which lead the trend of present work to follow the present data since their results where obtained through a standard procedures adopted by many other references. One of these standard steps is the calibration of five- hole probe without flow conditions based on two protractors for both yaw and pitch angles after making all the level adjustment for the rotating jig holder.

The measurements of the exit blade cascade flow field were carried out with the following objectives:

a) To obtain a better physical understanding of the evolution of secondary flow downstream of the blade passage.
b) To determine the characteristics of the blade cascade wake, including its movement path, the growth of its wake width, and the physical awareness of present problem.

A two-dimensional measurement grid was devoted for the region downstream of blade cascade starting from throat plane represented by the pitch distance. The mesh of planes parallel to the pitch plane were divided into ten mesh points with distance of (0.5 cm) while the planes perpendicular to the axial one were divided into eleven points with distance of (1 cm). Finally the grid points will have a mesh of (10 x 11).

Contour of velocity components

Refer to Figure-5, it can be noticed that the-upstream flow velocity of (19 m/s) will led to velocity rate of primary flow (u) for both reverse and forward flow. The amount of turbulent intensity through out blade passage and downstream of blade trailing edge was increased in accordance, which related to the additional fluctuation of wake flow region as the flow accelerated and increases its kinetic energy with existing of shear layer between regions that undergoes a reverse flow field against the forward flow regions. From other point of view, expanding of wake flow regimes to overlap the area above midpitch line may attributed to the effect of passage vortex, inviscid core region, trailing filament, and trailing shed vortices, which works as a continuous local source of momentum convection and surmount the regions with a positive velocity leading to large amount of momentum transfer between layers of both regions and finally rising the secondary flow velocity components (v) and (w) are shown in Figures 6 and 7, respectively. It can be seen from Figure-6 that for a downstream distance of one chord length, a pair of stagnation regions appeared to surround another region that posses negative and positive values of velocity equal to (-5, and -10 m/s). It is important to notice that the appearance of any flow region having velocity (v) other than zero will lead to the occurrence of secondary flow field. Same conclusion was implemented for the (w)

©2006-2012 Asian Research Publishing Network (ARPN). All rights reserved.

velocity component. Recalling the subject of momentum transfer between layers having highest potential energy and zero kinetic energy, the exchange of momentum rate among former mentioned regions will continued to reveal same trend of wake flow formation due to this rate of exchange. Moving forward to the second and third downstream axial distance having values of two and three times the chord length, the important note that can be raised from these locations of measurements was -the harmonization of their (v) flow field in comparison to their values in the (u) flow field. This harmonization can be sensed when a region with high reverse (u) flow or stagnation flow (i.e., u = 0 m/s) is represented in the (v) flow field by a high limit of secondary flow component (i.e., v) and this consolidates the vision of wake propagation downstream of blade cascade which posses more than one dimensional flow field component. Figure-7 shows the contour of z-axis velocity components (w), for the three recommended upstream velocity values. It is convenient to relate this component of velocity to the velocity in the y-axis (i.e., v component) since both of them will perform the plane of rotation that coincide with pitch plane, the plane at which the passage vortex and other former mentioned type of vortices. Finally, wake may still be felt several chords downstream and this are agreed well with [11].

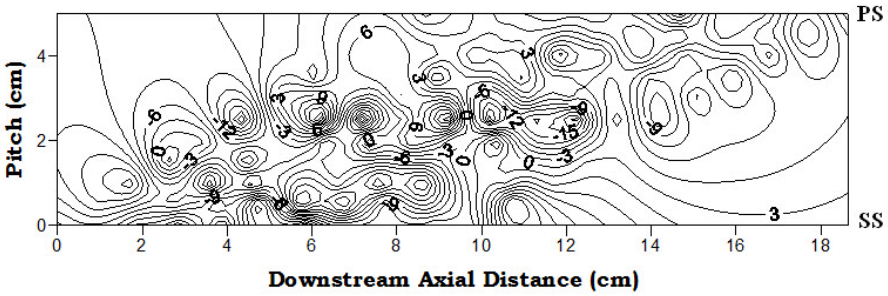

Figure-5. Velocity components [u, m/s] downstream of blade cascade.

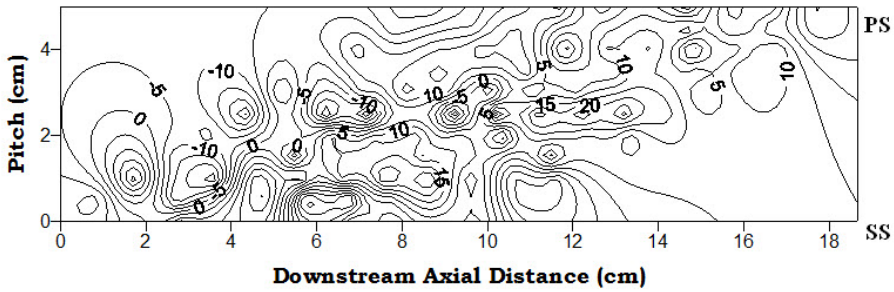

Figure-6. Velocity components (v, m/s) downstream of blade cascade.

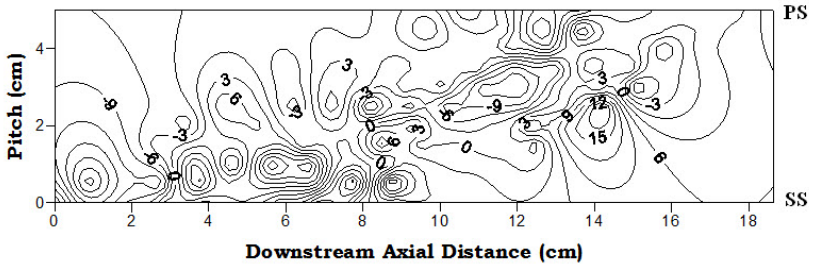

Figure-7. Velocity components (w, m/s) downstream of blade cascade.

Contours of pressure loss coefficient

The contour of total pressure loss coefficient is shown for different downstream distance in Figure-8. This trend represented by the formation of intermediate wake regime started just downstream of the trailing edge plane at which the center of traveling wake occurs at (0.1) of the pitch distance (s). However, this is not the only distinct feature of the present trend, but apparently this figure shows that the total pressure coefficient (Cpt) also manifest a region of propagating wake starts from the end of former mentioned wake center to almost twice chord length towards downstream direction with a pitch distance (s) equals to (0.75 s).

©2006-2012 Asian Research Publishing Network (ARPN). All rights reserved.

These high loss regions that represented by appearing of high regions of total pressure loss coefficients vary between (1.7 and 1.9). The maximum loss regions occur close to the suction surface. Losses increase as flow travels downstream of the blade cascade due to mixing of the wake, the decay of the vortices and the growth of the endwall boundary layer. The domination of wake region to almost all the area downstream of blade trailing edge can be related to the persistence of momentum exchange between layers of higher rate of velocities (i.e., higher rate of momentum) with those having low rate of velocities due to the decay of flow near suction surface which result at the end to the phenomena mentioned before. Reference [11] mentioned that the core of passage vortex is seen to migrate toward midspan and toward the middle of the passage as it flows downstream. This explanation validate the result of present study which manifest the concentration of wake region on midspan and almost up to middle passage distance represented by the pitch distance.

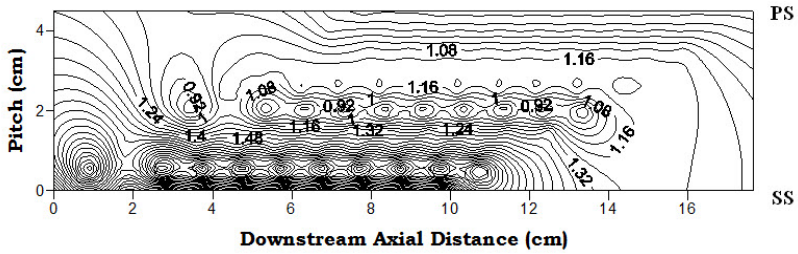

Figure-8. Total pressure loss coefficient (Cpt).

Contours of static pressure loss coefficient for a range of downstream axial distance are given in Figure-9. In this case study, it is batter to start discussion from the pressure side since this area experiences a common trend represented by occurring of static pressure regimes that show the constant lines of static pressure loss start to emerge after almost two third of blade chord but with increasing their density per pitch distance. The pitch wise variation of static pressure is much reveals in areas below mid pitch reference line with that above this reference. Rapid decay of the wake static pressure is conducted in the region lies below midpitch line.

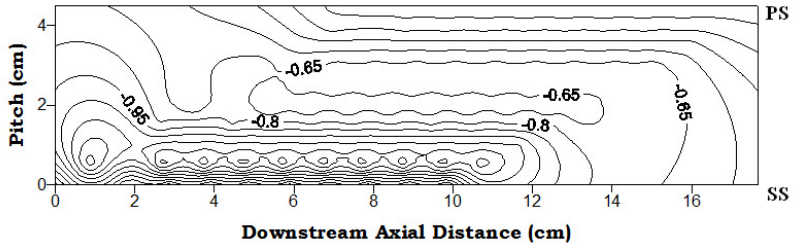

Figure-9. Static pressure loss coefficient (Cps).

The alteration of stagnation pressure loss coefficient (Yp) is shown in Figure-10. It can be noticed that in general they manifest a movable wake region transported in axial direction for a distance of (0.65%) from chord length downstream of trailing edge, and then starts to move in a diagonal direction from suction surface towards pressure surface. Bowing of the wake fluid is most evident in this Figure and originates near the trailing edge plane. The wake fluid convicts with the local velocity and distorts into the bowed shape. The velocities near the suction surface are higher than near the pressure surface and so fluid near the suction surface convicts through the passage more rapidly than the fluid near the pressure surface resulting in reorientation. This is most clearly seen by comparing the flow downstream of blade cascade at the trace line of suction surface in comparison with that of pressure surface. The difference in convection velocities also causes the wake segment to elongate and this in turn decreases the wake width to conserve the circulation of the wake fluid.

©2006-2012 Asian Research Publishing Network (ARPN). All rights reserved.

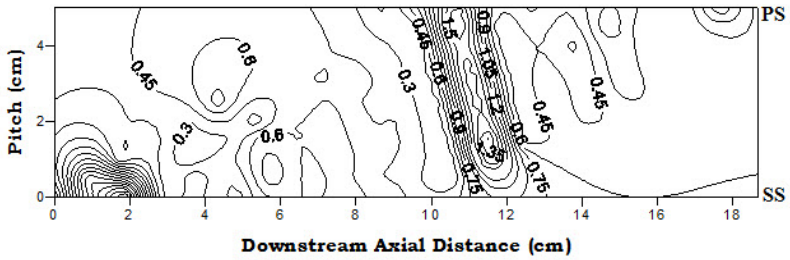

Figure-10. Stagnation pressure losses coefficient (Yp).

Contours of kinetic energy

Representation of total kinetic energy pertains to primary flow and secondary kinetic energy was shown in Figures 11 and 12, respectively. It can be seen that for an axial distance of two chord length, the secondary kinetic energy become the dominate part on account of total kinetic energy for almost all of the region lies inside that axial distance with a noticeable rise for the bulk of secondary energy from one velocity to another due to increase of turbulence intensity. After flow pass the reference of two-chord distance, the total kinetic energy starts to surmount that of secondary one since the flow tend to overcome the unsteadiness of flow by accounting on increasing the primary flow energy. Turbulence kinetic energy will then get dissipated by viscous action. This conclusion was also mentioned by reference [12].

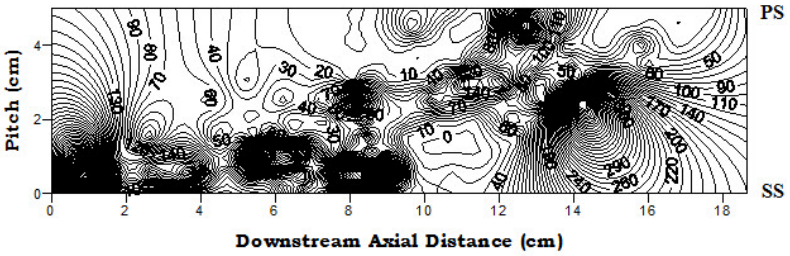

Figure-11. Total flow energy.

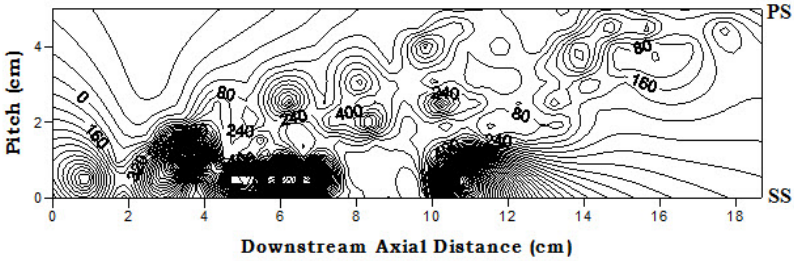

Figure-12. Secondary flow energy.

Maximum pressure loss coefficients

Figure-13 illustrate the variation of maximum (Cpt) in the axial downstream direction, in order to trace the path of maximum losses points. As mentioned in previous discussions for the part concerned with the contribution of secondary flow sources, inviscid core and wake formation. It can be noticed that the common trend revealed for (Cpt) max is the consecration of this parameter on a region located below mid pitch distance even if observer continued toward downstream direction. This trend became noticeable for all range of upstream velocities and lead discussion via the conclusion stated that the effect of combined three dimensional flow represented by passage vortex, inviscid flow region, trailing edge vortices, and all other losses sources still dominant in downstream direction even after it pass almost two chord length which validate the results listed in [l]. It mentioned that this type of losses (potential flow effect) will still be noticed even after two or three chord length while the inviscid flow will diminishes after a few distance downstream of blade cascade. Also the position of (Cpt) max starts from beginning on higher level up to 1.4 (c) and return to a lower position in downstream axial distance. Same behavior repeated for the position of maximum static pressure coefficient (Cp) max remains on same level for all the downstream axial distance. This trend for the locations of both (Cpt) max and (Cps) max

©2006-2012 Asian Research Publishing Network (ARPN). All rights reserved.

reveal the identical vision of all parameters discussed before.

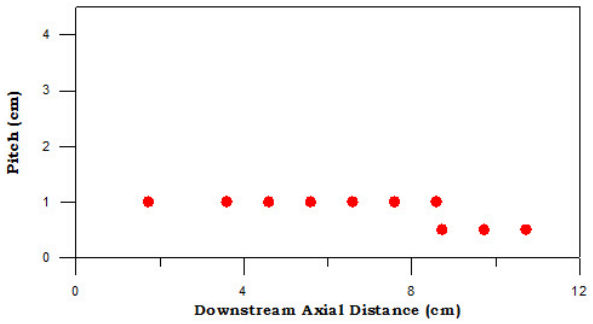

Figure-13. Position of maximum (Cpt).

CONCLUSION

The following conclusions are drawn from this study:

- The total pressure loss coefficient reflects the concentration of wake region on midspan and almost up to middle passage distance represented by the pitch distance, except for low range of upstream velocity;
- It was concluded that the stagnation pressure loss manifests regions of high losses at an axial distance of (0.45%) of the chord length while the regions distributed after and before this region posses lower values as the flow moving far from this point and vice versa; and
- It is found that the effect of combined three dimensional flow represented by passage vortex, inviscid flow region, trailing edge vortices, and all other losses sources still dominant in downstream direction even after it pass almost two chord length.

REFERENCES

[1] Dennis and Han Z. 1999. Constrained Shape Optimization of Airfoil Cascades Using a Navier-Stokes Solver and a Genetic/SQP Algorithm. ASME Paper No. 99-Gt-441.

[2] Pritchared L. J. 1985. An Eleven Parameter Axial Turbine Airfoil Geometry Model. ASME Paper No. 85-GT-219.

[3] Sawyer J. 1979. Chapter 4. Sawyers Gas Turbine Engineering Hand book. 2nd Edition. Vol. I. Gas Turbine Publications, Inc. Stamford, Conference. p. 70.

[4] Ghaly W. and T. Mengistu. 2003. Optimal Geometric Representation of Turbomachinery Cascade using NURBS. Journal of Inverse Methods in Engineering, in press.

[5] Prey L. Miller I V and David P. Miller. 1995. Blade CAD, an Interactive Geometric Design Tool for Turbo machinery Blades.

[6] Riyadh Abraham. 2004. Design Construction and Calibration of 90° Conical Pressure Five Hole Probe. M. Sc Thesis.

[7] Bosman C. and Highton J. 1979. A calibration Procedure for three Dimensional, Time Dependent, Inviscid Compressible Flow through Turbomachine Blades of any Geometry. J. of Mech. Eng Science. 21: 39-49.

[8] Charley Fleischmann. 2002. Measurement of Hot Gas Flow in a Fire Compartment. M. Sc Thesis. University of Compartment.

[9] Sitaram N., Lakshminarayana B and Ravindranath A. 1981. Conventional Probes for the Relative Flow Measurement in a Turbomachinery Rotor Blade Passage. ASME Journal of Engineering for Power. 103: 406-414.

[10] Barker K.W., Gallington R.W. and Minister S.N. 1979. Calibration of Five-Hole Probe for online Data Reduction. USAFA- TR-79-7.

[11] Langeston. 2001. Secondary Flow in Cascades. ASME Journal of Turbomachinery.

[12] Gregory Smith and Graves CP. 1988. Growth of Secondary Losses and Vortices in an Axial Turbine Cascade. ASME Journal of Turbomachinery. 110: 1-8.